Investigation of particle velocity in FCC gas-fluidized beds based on different measurement techniques

Tebianian, Sina; Dubrawski, Kristian; Ellis, Naoko; Cocco, Ray A.; Hays, Roy; Reddy Karri, S.b.; Leadbeater, Thomas W.; Parker, David; Chaouki, Jamal; Jafari, Rouzbeh; Garcia-trinanes, Pablo; Seville, Jonathan P.k.; Grace, John R.

DOI:
10.1016/j.ces.2015.01.049

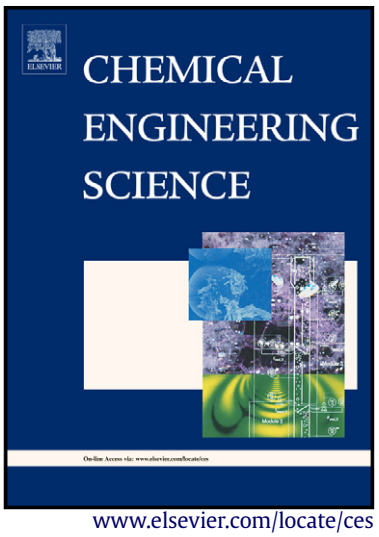

www.elsevier.com/locate/ces

Investigation of particle velocity in FCC gas-fluidized beds based on different measurement techniques

Sina Tebianian, Kristian Dubrawski, Naoko Ellis, Ray A. Cocco, Roy Hays, S.B. Reddy Karri, Thomas W. Leadbeater, David J. Parker, Jamal Chaouki, Rouzbeh Jafari, Pablo Garcia-Trinanes, Jonathan P.K. Seville, John R. Grace

PII: S0009-2509(15)00078-0
DOI: http://dx.doi.org/10.1016/j.ces.2015.01.049
Reference: CES12142

To appear in: *Chemical Engineering Science*

Received date: 20 December 2014
Revised date: 19 January 2015
Accepted date: 23 January 2015

Cite this article as: Sina Tebianian, Kristian Dubrawski, Naoko Ellis, Ray A. Cocco, Roy Hays, S.B. Reddy Karri, Thomas W. Leadbeater, David J. Parker, Jamal Chaouki, Rouzbeh Jafari, Pablo Garcia-Trinanes, Jonathan P.K. Seville, John R. Grace, Investigation of particle velocity in FCC gas-fluidized beds based on different measurement techniques, *Chemical Engineering Science,* http://dx.doi.org/10.1016/j.ces.2015.01.049

Investigation of particle velocity in FCC gas-fluidized beds based on different measurement techniques

Sina Tebianian[1,✉], Kristian Dubrawski[1], Naoko Ellis[1], Ray A. Cocco[2], Roy Hays[2], S.B. Reddy Karri[2], Thomas W. Leadbeater[3], David J. Parker[3], Jamal Chaouki[4], Rouzbeh Jafari[4], Pablo Garcia-Trinanes[5], Jonathan P. K. Seville[5] and John R. Grace[1]

[1] *Department of Chemical and Biological Engineering, University of British Columbia, Vancouver, Canada V6T 1Z3*

[2] *Particulate Solid Research, Inc. (PSRI), Chicago, IL, United States 60632*

[3] *Positron Imaging Centre, University of Birmingham, Birmingham, United Kingdom B15 2TT*

[4] *Département de génie chimique, Ecole Polytechnique, Montréal, QC, Canada H3T 1J4*

[5] *Department of Chemical and Process Engineering, University of Surrey, Guildford, Surrey GU2 7XH, UK*

Abstract

The novel traveling fluidization column, designed and built to assure identical operating conditions, was deployed to compare alternate experimental measurement techniques for hydrodynamic characterization of gas-fluidized beds. This paper compares measurements of particle velocity obtained by radioactive particle tracking (RPT – non-invasive at the Ecole Polytechnique), positron emission particle tracking (PEPT – non-invasive at University of Birmingham), optical fibre probes (invasive at UBC) and borescopic high speed particle image velocimetry (invasive at PSRI) carried out with FCC particles of mean diameter 107 μm. All of the techniques provided similar trends with respect to time-average particle velocity profiles, but significant differences were observed in some cases. Analysis of the results, focusing on the physical principles of each measurement technique, provides valuable insights into the reasons for the observed discrepancies. The results also add to a unique hydrodynamic database for validation of CFD and other mechanistic models.

Keywords: Fluidized beds; Particle velocity; Optical fiber probes; Borescopic PIV; Radioactive Particle Tracking; Positron Emission Particle Tracking

✉ Corresponding author, Email: stebianian@chbe.ubc.ca, sinatebian@gmail.com, Phone: (604)8273178

1.0 Introduction

Gas-fluidized beds are used extensively in industrial applications because of their unique features such as excellent heat transfer, ease of solid handling, ease of particle processing and efficient solid mixing. Despite the extensive efforts of many researchers and practicing engineers, design and scale-up of gas-fluidized beds are still challenging, often relying on empirical correlations (Yang, 2003). As a result, fluidized beds are commonly eliminated from consideration as this uncertainty compromises the risk tolerances in the corporate culture. Lack of fundamental knowledge and accurate experimental data leading to valid hydrodynamic models are among the factors that cause uncertainties with design and scale-up. Mechanistic models based on computational fluid dynamics (CFD) hold great promise for the design and understanding of gas-fluidized beds. However, as reported by Grace and Taghipour (2004), validation of hydrodynamic models requires comparison of predictions with an extensive array of experimental data, with due appreciation of their accuracy.

Solid motion is of extreme importance as it influences many aspects of gas-fluidized bed performance:

- In fluidized bed reactors, vertical movement of solid particles can transport reaction components and catalysts upward and downward in the bed, affecting axial dispersion, conversion and selectivity (Kunii and Levenspiel, 1991; Nguyen et al., 1977).
- Many processes involve contact between solids with different densities (e.g. in the production of titanium or zirconium, drying of solids). Solids movement and velocity influence mixing processes and staging of the solids.
- Erosion of in-bed tubes and other components in fluidized beds, as well as particle attrition, are directly related to particle motion, affecting the velocity and frequency of

impact (Lyczkowski et al., 1993).

- Favourable heat transfer coefficients in fluidized beds are due to the convective movement of solids around and along immersed surfaces.

Various invasive and non-invasive experimental techniques have been proposed for the hydrodynamic study of fluidized beds [6–8]. However, except for our recent voidage data (Dubrawski et al., 2013), the accuracy of many of these techniques has not been verified by comparing results obtained by alternative techniques under identical operating conditions. This makes it difficult to investigate the merits and reliability of each measurement technique.

In the present study we extended the reporting of results from the novel traveling fluidized bed (TFB), designed and built to provide identical operation in different physical settings and allowing direct comparison of alternate experimental measurement techniques (Dubrawski et al., 2013). Operating with the same equipment, with the same particles and under the same experimental conditions eliminates differences due to discrepancies between equipment, particles and operating conditions as sources of variation in data.

In our previous work (Dubrawski et al., 2013), radial profiles of time-average voidage measured by three different optical probes, electrical capacitance tomography, X-ray computed tomography and radioactive particle tracking were compared. This paper extends this study to compare different techniques for the measurement of another important hydrodynamic parameter, particle velocity.

Four different experimental techniques – radioactive particle tracking (RPT) a non-invasive method practised at the Ecole Polytechnique, Positron emission particle tracking (PEPT), a non-invasive technique developed at the University of Birmingham, optical fibre probes, an invasive technique deployed at the University of British Columbia (UBC), and borescopic high-speed

particle image velocimetry (PIV), an invasive measurement method owned by Particulate Solid Research Inc. (PSRI) – are employed to investigate particle vertical motion in the traveling fluidized bed. Radial profiles of time-average particle velocity and the probability distribution function of solid velocity obtained by all four techniques are directly compared. This paper reports the results from the experiments using FCC particles. Results of solid motion obtained from the TFB operated with sand particles will be presented in a separate paper. Analysis of the profiles obtained by the four techniques leads to valuable insights into the physical principles characterizing each measurement method that underlie, at least in part, the discrepancies between the solid velocity profiles obtained from the four techniques. The results reported in this study, together with the earlier data (Dubrawski et al., 2013), constitute a comprehensive hydrodynamic database for validation of CFD and other mechanistic models.

2.0 Experimental

The experimental apparatus consists of a novel fluidized bed unit, its support structure, basic instrumentation and auxiliary components, all of which traveled with the FCC catalyst (d_{sauter} = 107 μm, ρ_p = 1560 kg/m^3) and silica sand (d_{sauter} = 292 μm, ρ_p = 2644 kg/m^3) particles and the first author to different research laboratories for experimentation using different sophisticated instrumentation. The column has a 0.96 m long x 0.133 m i.d. dense bed section, surmounted by a 1.36 m long x 0.190 m i.d. freeboard section, as shown in Figure 1. An internal cyclone is employed to capture the entrained particles and re-insert them in the dense bed. The gas flow rate is measured using an array of sonic nozzles adequately calibrated against an orifice flow meter. The fluidizing gas passes through a perforated distributor plate containing 49 perforations of 2.5 mm diameter arranged on a circular pattern. Other details of the traveling column, particles and

operating conditions are provided elsewhere (Dubrawski et al., 2013).

A brief description of the measurement techniques relevant to this paper is given below. The Nyquist criterion of sampling frequency, considering that the system is characterized by a prevalent frequency of 3-5 Hz, was largely respected for all measurement techniques. The sampling periods of each measurement technique provided enough data to produce reasonable reproducibility as indicated in the Results section.

2.1 Optical Fibre Probes

An optical probe with a fibre cross-sectional dimension similar to the particle diameter has been used at UBC to measure the local velocity of passing solids by cross-correlating two light-receiving signals, as described by Ellis (2003) and Liu et al. (2003). Measurements were obtained at three different heights, at each of which the probe was inserted from ports located on the column perimeter to measure the solid velocity at different radial locations along a diameter.

To calibrate the probe, as reported by Liu et al. (2003), a disc with a particle affixed was rotated at a known angular velocity, with a three-fiber probe aligned parallel to the direction of particle motion, simulating the movement of particles in the bed. A stepper motor and optical encoder were used to precisely control the rotation speed. Over a range of known linear velocities, using a cross-correlation method, the time-lag between pairs of signals allows the effective distance (L_e) between receiving ends of the probe to be determined. The effective distance and time lag (τ_l) determined from cross-correlation of experimental data give the velocity of particles passing the fibres (v_p) as:

$$\begin{cases} (a) v_p = L_e / \tau_l \\ (b) \tau_l = M \times 1/f \end{cases} \quad (1)$$

where f is the sampling frequency and M is a positive integer which, when multiplied by the inverse of the frequency, gives the time lag between the two signals. It is clear that τ_l is a discrete function of the frequency.

Table 1 **– Optical probe properties**

Unit	PV-4A	**Measurement heights**	3 (z = 0.24, 0.40 and 0.56 m)
Probe type	Cross section similar to d_{sauter}	**Sampling time, s**	40 (80 × 0.5 s intervals)
Probe specifications	3-fibre parallel d_{probe}: 4 mm d_{fibre}: 280 μm	**Sampling frequency, kHz**	15.6 (wall region) 62.5 (other positions)
Glass window	Yes	L_e**, mm**	0.38
Integration period, s	0.13 (wall region), 0.033 (other positions)	**Cross-sectional positions**	7

Table 1 reports the properties of the optical probe employed in this study. Sampling frequency and integration period are important parameters for obtaining accurate solid velocity values. Their choice is dictated by the necessity of capturing instantaneous values of particle velocity within a certain range of measurable values, according to the following equations (Liu et al., 2003):

$$\begin{cases} (a)\left|v_{p,min}\right| = 2L_e \big/ T_{int} \\ (b)\, f_{min} = \dfrac{v_{p,max}\left(v_{p,max} - E\right)}{L_e \cdot E} \end{cases} \tag{2}$$

where $v_{p,min}$, $v_{p,max}$, T_{int} and f_{min} are minimum and maximum measurable particle velocity, integration time and required sampling frequency, respectively, for determining the maximum velocity with a certain accuracy. The parameter E represents the error, defined as the difference between two neighbouring points close to the maximum cross correlation (Herbert et al., 1994), dictating the accuracy in determining the maximum solid velocity. High particle velocity

corresponds to low τ_l, and therefore to low M, as given by Equation (1). Equation (1) indicates that the higher the sampling frequency, the bigger the multiplicand (M) corresponding to the time lag of a high velocity particle, resulting in an increase of the number of points near the maximum cross-correlation coefficient and lower error (E).

A short T_{int} corresponds to a high $v_{p,min}$; yet, if integration time is too long, no instantaneous velocity is detected since the signals would result from multiple particles moving with different velocities. For most radial positions a sampling frequency of 62.5 kHz was deployed. The exception was the region close to the column wall, where, because the velocities were smaller in magnitude, a lower frequency of 15.6 kHz was used. Continuous data acquisition for 40 s was not compatible with the capabilities of the computer in use; therefore, the data were collected during 20 intervals of 2.09 s for the wall region (r/R = 0.83) and 80 × 0.52 s intervals for all other radial positions. Each interval was then divided into 16 sub-intervals that represent the integration time over which the signals were cross-correlated (Table 1).

The obtainable magnitude of velocities with a maximum tolerance for error (E) of 10% for the wall region are included in the interval I_w = [0.0058 m/s, 0.66 m/s] and for the other radial positions in the interval I_p = [0.023 m/s, 2.64 m/s]. The time lag corresponding to the maximum cross-correlation coefficient is used to calculate the velocity of particles passing the probe tip. Solid velocities corresponding to a maximum cross-correlation coefficient greater than 0.5 are considered to be valid (Liu et al., 2003).

In order to obtain a valid cross-correlation, the particles must move almost vertically in the measurement volume of the optical probes. If a particle is moving with too great a deviation angle with respect to the vertical direction, it is not detected in the second fibre field of view, and no valid cross-correlation is then possible. The maximum deviation angle for which the particle

movement is traceable by the optical probe is extremely important for direct comparison of the results with other measurement techniques. For this purpose, experiments were carried out where the particles were poured vertically in front of the optical fibre probe mounted with different deviation angles with respect to the vertical direction. The cross-correlation success at different deviation angles was quantified by considering the percentage of the data that present a maximum cross-correlation coefficient greater than 0.5. Figure 2 shows that for FCC particles there is a sharp decrease in the percentage of valid velocity vectors for angles of deviation to the vertical exceeding 30 degrees.

2.2 Borescopic High Speed Particle Image Velocimetry (PIV)

A high-speed borescopic PIV system, owned and operated by Particulate Solid Research Inc. (PSRI), was deployed to investigate the solid motion in the fluidized bed. Details of the borescope can be found in Cocco et al. (2010). The PIV system utilizes a high-speed, high-resolution Phantom v7.3 camera with a resolution up to 800 x 600 pixels. The capture rate was 3000 frames/s, with an exposure time of 10 μs. This rate was high enough to capture the highest particle velocities in the system. With a custom 6 mm borescope, it was possible to perform high-speed PIV measurements at different radial and axial locations inside the fluidized bed. This novel technique facilitates optical access to the interior of a dense fluidized bed, which is otherwise impossible due to the opacity of the system.

The total sampling period of the high-speed PIV was chosen considering the number of data that had to be produced, memory required for their storage and the time needed for analysis. With axial-symmetry assumed for each measurement location, the total sampling period was 10 s, resulting from 10 one-second intervals of continuous acquisition. Each video corresponding to 1

s of data sampling occupied 0.5 GBytes of memory. The sampling rate should be at least two times bigger than the Nyquist frequency in order to capture the typical hydrodynamic phenomena in the dense bed which is characterized by a prevalent frequency of 3-5 Hz. Properties of the borescopic high-speed PIV system are summarized in Table 2.

Table 2 – Borescopic high-speed PIV system properties

Camera	Phantom v7.3	**Measurement heights**	3 (z=0.24, 0.4 & 0.56 m)
Frame rate	3000 frames/s	**Sampling time**	10 (10×1 s intervals)
Camera resolution	256×256 pixels	**Borescope diameter**	6 mm
Exposure time	10 μs	**Region of interest**	1.5 × 1.5 mm
Cross-sectional positions	9	**Glass window**	Yes

A Xeon light and an oil filled light pipe funnelled intense light to the tip of the borescope to illuminate the particles and generate high-quality images. In order to prevent particles from blocking the illumination source, a glass window was mounted in front of the borescope.

FCC catalyst particles are characterized by substantial electrostatic forces which can cause particles to adhere to the tip of the borescope, blocking the view of the solid motion. Significant improvement was obtained by rubbing the borescope tip with an antistatic sheet used mainly for dryers every 2-3 runs, largely preventing particle adhesion.

The analysis of the high-speed PIV data consisted of conversion of the videos into consecutive grayscale images and determination of solid displacement for each pair of consecutive images using an open source Matlab code called PIVlab, developed by Thielicke and Stamhuise (2013), where the particle velocity is determined using a multiple pass interrogation method, based on a grid refining scheme described by Raffel et al. (1998). The following points summarize the main steps for calculating the solid displacement from consecutive frames:

1. A region of interest of about 2 × 2 mm was chosen. A mask was used to prevent interference from outside regions.

2. A large interrogation area capable of capturing the greatest particle displacement within the region of interest was chosen.
3. A standard interrogation was performed based on the cross-correlation peak detection from successive images.
4. The results of Step 3 were used as estimates for the next higher resolution level. The estimated displacement data were projected onto the next smaller interrogation area, and this procedure was repeated until the final image resolution was reached.
5. Each velocity vector refers to the displacement of the particles present in a dimension equal to the smallest pass at a certain position.
6. In regions where no particles are present, the software assigned a "Not a Number" (NaN) velocity value which is then ignored in time averaging. The results containing the instantaneous velocity vectors and the relative positions were saved into consecutive text files. Velocities more than three standard deviations from the mean were removed.
7. A Matlab code was then used to calculate the time-average velocity at each radial position. As with RPT and PEPT, two values were calculated, one averaging the vertical component of all measured velocities and the other where only values with a deviation angle with respect to the vertical direction less than 30° were included, in order to compare with the optical probe data.

The choice for the final interrogation pass size depends on the particle image density. Below a certain number of particles present in the pass (typically N<4), the displacement detection rate decreases significantly, as pointed out by Raffel et al. (1998). Figure 3 shows an image analyzed by PIVlab and a corresponding velocity map. The vectors are present only in the region of interest where the image is in focus.

2.3 Radioactive Particle Tracking (RPT)

Details of the principles of RPT and the equipment used in this study can be found elsewhere (Dubrawski et al., 2013; Larachi et al., 1996). A single radioactive tracer particle was introduced into the fluidized bed, and an array of NaI gamma-ray detectors surrounding the column at different heights were calibrated to locate this tracer particle at different positions covering the entire volume of the column as a function of time. Pure scandium, obtained from Alfa Aesar, was chosen as the tracer particle. Samples were cut mechanically under magnification to provide the particle sizes of interest. The samples were irradiated to 200 μCi at McMaster University in Hamilton, Ontario. Since pure scandium has a density of 2990 kg/m^3, the tracer was immersed in epoxy resin (density ≈ 750 kg/m^3) post-irradiation to decrease the net particle density, in order to better match that of the experimental particles. It was found that tracer particles smaller than 400 μm could not be handled safely. Thus, single tracer particles from the same batch were used for both the FCC and sand particles. Scandium particles as small as ~250 μm in diameter were dipped in epoxy, making nearly spherical tracer particles of ~400 μm diameter, with a composite density of ~2000 kg/m^3. Physical properties of the tracer particle are compared to those of the bed material in Table 3.

Table 3 – Comparison of the bed material and the RPT and PEPT tracer particle physical properties

	FCC	**PEPT Tracer**	**RPT Tracer**
d_{sauter} **(μm)**	107	100	400
ρ_p **(kg/m^3)**	1560	1100	2000
Shape	Nearly spherical	Perfectly spherical	Nearly spherical

The 3-D coordinates (x,y,z) of the tracer during the RPT tests, were determined as a function of time. The duration of each test was 4 hours, whereas the time interval between each successive data acquisition (Δt) was 10 ms. Each test was repeated, yielding a total sampling period of eight

hours. The radial profile of particle velocity was correlated at the same measurement heights as those obtained from optical probe and borescope using a Matlab code. The most important steps for correlating the radial profiles include:

i. The tracer position coordinate matrix was fed into the program, with the instantaneous particle velocity calculated from successive positions of the tracer particle as:

$$v_p = \begin{bmatrix} v_{p,x} \\ v_{p,y} \\ v_{p,z} \end{bmatrix} = \begin{bmatrix} \frac{x_{i+1} - x_i}{\Delta t} \\ \frac{y_{i+1} - y_i}{\Delta t} \\ \frac{z_{i+1} - z_i}{\Delta t} \end{bmatrix} \quad (3)$$

ii. When and only when the tracer crosses a specific measurement level, the coordinates of the tracer particle were saved. Velocity components were then calculated from successive positions. Outliers more than 3 standard deviations from the mean were filtered out.

iii. Two types of averaging were conducted. With the first type, the vertical components of velocity of all particles crossing the plane of interest were averaged. In the second type, only the velocity vectors with small deviation angles (< 30°) with respect to the vertical direction were considered in order to provide direct comparison with the optical probe data, and

iv. The column cross-sectional area was divided into five concentric areas. The velocity vectors of the tracer crossing each measurement plane with its centre inside each of the concentric areas were counted and averaged.

The volume-based algorithm commonly used for determining the solid motion pattern in the fluidized bed from particle tracking techniques, divides the column into a mesh consisting of

small cells of finite volume (e.g. 30×30×30 mm) and calculates the local time-average velocity, for the tracer velocity every time that it occupies a certain cell during the entire data sampling period (Larachi et al., 1996). In this study, however, the crossing-level algorithm indicated in points (i-iv) was mainly employed due to the following factors:

- The particle tracking data should be as comparable as possible to those obtained by the invasive techniques in terms of the measurement volume. The optical probe and the borescope produce essentially zero-volume point measurements at the levels of interest and the condition (ii) stated in the algorithm produces a similar measurement volume corresponding to a zero-width plane.
- If instead of requiring the condition (ii) stated above, we calculate the velocity of the tracer when it is present in an annulus of a finite (30 mm) vertical dimension, the number of velocity vectors increases substantially. However, considering a certain region, since the slowly moving particles spend more time therein compared to the high velocity ones, the time-average solid velocity is biased towards the low velocity vectors. This condition is totally absent in optical probe data since the velocity vector corresponding to a certain particle is calculated exclusively once due to the cross-correlation criteria.

The borescopic analysis has a slight tendency to count extremely low-velocity vectors more than other ones. This condition applies mostly to nearly-zero velocities since the moving particles spend a very short time in the small measurement volume of the borescope.

The centre of the distributor plate was chosen as the origin of the coordinate system. The relative positions of the detectors are reported in our previous work (Dubrawski et al., 2013).

2.3 Positron Emission Particle Tracking (PEPT)

Positron emission particle tracking (PEPT), similar to RPT, allows non-invasive observation of a single radioactive tracer particle within the domain of the fluidized bed. The physical principle of PEPT differs slightly from RPT since the radioactive particle contains neutron-deficient nuclei that undergo β-decay accompanied by positron emission. Any positron emitted by β-decay combines with its antiparticle (electron) generating two back-to-back 0.511 MeV γ-rays. The difference in emission mechanism which is based on single photon emission for RPT and dual photon emission for PEPT affects the method of detection and arrangement of sensors for particle tracking (Larachi et al., 1996). Details of the experimental apparatus for tracer localization are given elsewhere (Leadbeater et al., 2012; Stein et al., 1996). This paper summarizes the main ideas behind the algorithm for tracer particle tracking which are important for the interpretation of the results.

Simultaneous detection of gamma photons resulting from positron annihilation defines a trajectory called Line of Response (LoR). The position of the annihilation site must in principle lie along the LoR. Ideally, the position of a stationary particle can be detected from the intersection point of only two LoR's. However, some detected events are corrupt (due to scatter, random coincidences, etc.). The PEPT algorithm rejects these corrupt events and determines the location of the tracer particles based upon the remaining set of LoR's.

Starting with a small set of LoR's, N, the minimum distance point, m_s, was then calculated as the point in space that minimizes the sum of perpendicular distances of the LoR's present in the initial set. This point was considered as the first estimate of the tracer position. Trajectories that lie furthest from m_s were assumed to be corrupt and were removed from the set. The minimum distance point was then re-evaluated from the new set of LoR's. This iteration process continued

until a predefined fraction, f_{opt}, of the sample N remains. The final m_s position was calculated from the last fraction of N ($f_{opt} \times N$) with a precision Δ given by the average perpendicular distance from this point to each LoR in the final set. For a stationary particle, Δ is given by the following equation (Leadbeater et al., 2012):

$$\Delta = \frac{w}{\sqrt{f_{opt} N}} \tag{4}$$

where w is the spatial resolution of the detection camera, measured to be around 8 mm. The magnitude of f_{opt} depends on the proportion of corrupt events; its optimal value was measured for each system using a stationary tracer (Leadbeater et al., 2012). For the TFB tests, an optimum fraction f_{opt} = 0.12 was used as the value that minimizes the standard deviation of the tracer location. From Equation (4) it can be observed that for a stationary particle, as expected, the larger the sample, the smaller the error in tracer location. With moving tracers, the LoR's in each set of events are spread along the particle trajectory. Therefore, the final set of LoR's does not converge into a single point, but surrounds a volume around the minimum distance point given by precision Δ. The value of N must be reduced for moving tracer particles to deal with the effect caused by movement. An exact theoretical argument for optimising N as a function of particle speed has not been found (Leadbeater and Parker, 2013).

In this study for each operating condition, the system was operated for a total of 3.5 hours comprising three 1-hour runs and a final run lasting 30 minutes. For each experimental run, the average coincidence rate, i.e. rate at which both pairs of gamma photons are simultaneously detected, was noted. Assuming that the uncertainty in location for a moving particle follows the same formalism as for a stationary particle, Δ was calculated for different values of N. Small values of N result in more detected positions of the moving tracer, but may result in a significant

decrease in location precision due to lack of enough LoR's for the calculation. High *N* provides enough LoR's for the particle location, but may decrease the precision due to a substantial movement of the tracer particle during the time defined by the set size. In this study, the initial sample size was chosen considering that its value should result in a reasonable localization rate and that the distance travelled between the successive locations be greater than 2Δ (where Δ is obtained from Equation (4)) for all tracer velocities greater than 0.01 m/s. Data for which Δ was larger than three times the standard deviation of the location uncertainties were discarded. The analysis of the raw data was performed using overlapping sets to increase position sampling, with each set of LoR's starting one fifth of the way through the previous set (Stein et al., 1996). Once the raw data were analyzed with specific criteria given by the input parameters such as *N*, f_{opt} and number of overlapping sets, a matrix with instantaneous spatial position of the tracer particle and the location precision was generated. From the successive positions, an instantaneous tracer particle velocity was measured. For overlapping sets, the tracer particle velocity was obtained by comparing eleven consecutive locations and performing a weighted rolling average of six estimates of the resulting velocities:

$$\overrightarrow{v_p} = 0.1\left(\frac{\vec{P}_{i+5}-\vec{P}_i}{t_{i+5}-t_i}\right)+0.15\left(\frac{\vec{P}_{i+4}-\vec{P}_{i-1}}{t_{i+4}-t_{i-1}}\right)+0.25\left(\frac{\vec{P}_{i+3}-\vec{P}_{i-2}}{t_{i+3}-t_{i-2}}\right)+ 0.25\left(\frac{\vec{P}_{i+2}-\vec{P}_{i-3}}{t_{i+2}-t_{i-3}}\right)+0.15\left(\frac{\vec{P}_{i+1}-\vec{P}_{i-4}}{t_{i+1}-t_{i-4}}\right)+0.1\left(\frac{\vec{P}_i-\vec{P}_{i-5}}{t_i-t_{i-5}}\right) \quad (5)$$

where $\overrightarrow{v_p}$ and $\vec{P}_i$ represent the particle velocity and location at instant t_i. The rest of the algorithm for determining the profile of time-averaged solid velocity at each operating condition was exactly the same as that for RPT. For RPT, equation (3) was preferred to the weighted rolling average method used for PEPT since the RPT sampling rate was fixed and, in certain

cases, much slower than for PEPT. Therefore, equation (7) could result in loss of instantaneous information for RPT. Nevertheless, 6-point averaging was tested for RPT, but it did not result in any improvement of the results in terms of comparison with the other data analysis techniques.

FCC particles could not be activated enough for the PEPT experiments. Therefore, Dowex SBR strong base (OH- form) anionic exchange resin beads whose properties are given in Table 3 were used as the tracer particle. The tracer particle then matched well the average size of the FCC particles, but the particle density was significantly lower.

3.0 Results

Radial profiles of time-average particle velocity obtained by all four experimental techniques are reported in Figures 4 to 11. Axial-symmetry is assumed for the data in each of these figures. The borescope, PEPT and RPT results in these plots result from considering two cases: (a) only the velocity vectors associated with solid motion with a deviation angle with respect to the vertical direction of 30 degrees or less (Figures 4-7); and (b) the vertical component of all velocity vectors of particles that crossed the measurement height (Figures 8-11). The lines connecting the data points, obtained by spline interpolation, are merely intended to facilitate the distinction of the results associated with different measurement techniques and should not be considered to be accurate interpolations of data between the measurement points. Therefore, caution must be taken into account when considering the experimental profiles for CFD models validation. Even though all the measurement heights were included inside the field of view of the PEPT camera, solid velocity results obtained by PEPT at 0.24 m above the distributor were excluded from the graphs since these results failed to satisfy the physical constraint that, for a steady-state measurement, the technique must produce a nearly-zero time-average solid mass flux over the

whole cross-section due to mass conservation.

Radial profiles provided by each of the four techniques show upward solid velocity at the centre of the column due to the solid movement induced by the wakes and drift caused by rising voids, accompanied by corresponding downward velocities near the wall. Agreement between the time-average solid velocity profiles obtained by the four techniques is no better than fair, with significant differences in some cases, especially between PEPT and the other three experimental techniques. In most cases PEPT produced downward velocities of the highest magnitude compared to the other techniques in the wall region (up to 8 times greater) and, to a lesser extent in some cases, highest upward velocities in the core region (up to 3 times greater).

The discrepancy between the results was quantified by calculating the absolute percent deviation of each technique result from the average obtained considering the results produced by all measurement methods at each superficial gas velocity and each spatial position. For each superficial gas velocity, the overall deviation of single techniques results from the mean value was calculated by averaging the deviations obtained at all spatial positions, and the results are given in Figure 12 for both filtering criteria. It can be observed that PEPT presents the highest magnitude deviation, optical probe the smallest, with RPT and borescopy somewhere in between. The error bars for the RPT, borescopy and optical probe represent 90% confidence intervals obtained by considering the whole sample of velocity vectors. For PEPT, since the location precision was given for each instantaneous tracer position, the uncertainty in the solid velocity was determined using the error propagation formula based on the coefficients in Equation (5). The resulting error bars for PEPT are based on the average value of velocity uncertainty. Even if the average value of velocity error for PEPT is reasonable (due also to the six-point-averaging method), it should be noted that the standard deviation of the error is substantial, leading to

uncertainties up to 0.2 m/s.

The best statistical reproducibility was delivered by the borescope which provided a large amount of data, producing nearly zero-width confidence intervals for all measurements. RPT, PEPT and optical probe provided larger, but reasonable, average confidence intervals, in the range of 10-20%.

The data collected by the borescope for periods of 10 and 15 s are compared in Figure 13. These results indicate that the experiments are not very sensitive to the duration of the sampling time.

In many cases, the radial profiles of particle velocity derived from the RPT, PEPT and borescopic techniques changed as a result of considering the vertical component of the tracer velocity when it crossed the measurement plane, rather than its velocity when it travelled with a small deviation angle with respect to the vertical direction. In some cases, the agreement between the results from these three techniques and the data from the optical probes was slightly better when all vertical components were considered.

For RPT, the count number, defined as the number of times the tracer was detected in a certain defined region, changed significantly with the radial position, but to a minor extent with the filtering criteria. PEPT count number appears also to have been nearly insensitive to the filtering criteria. Both techniques provide the lowest count numbers in the core of the bed which is expected due to the presence of voids moving mainly in the centre of the column resulting in smaller probability for the tracer particle to be present in that region compared to others. The count number would decrease if, instead of considering the vertical components of all velocity vectors, 30 degree deviation at most from the vertical was included as a data filtering criterion. However, as shown in Figure 14, sufficiently big count number was obtained for both particle tracking techniques, even with the 30° angle from the vertical included as a filtering criterion.

Probability distribution functions (PDF) of the solid velocity at different positions obtained by each measurement technique are plotted in Figure 15. Note that for all cases, there was remarkable similitude between the PDFs of the two non-invasive techniques (RPT and PEPT). The PDFs of solid velocity obtained by the borescope were slightly shifted towards lower magnitude velocities, producing a different shape compared to the PDFs of the other techniques in most cases. The PDFs of solid velocity from the optical probe were generally more similar to those produced by the non-invasive techniques.

Figure 16 reports the effect of exclusion of those velocities close to zero, not detected by the optical fibre probe, on some time-average radial profiles of particle velocity obtained by borescope, PEPT and RPT presented in Figures 4-7. This additional filtering, however, had a negligible effect on the reproducibility and statistical significance of the data since sufficient data points were still available for all of the techniques deployed.

4.0 Discussion

Consideration of the unique intrinsic characteristics and data processing methodologies associated with each of the four measurement techniques helps to explain some of the quantitative differences in the data provided by them. Measurement factors which contributed to the differences include the following:

- The optical probe and borescopic probe are both intrusive, and therefore interfere to some extent with the flow field being measured, the nature and extent of the interference depending on such factors as probe shape, size, orientation and roughness, as well as the prevailing direction, velocity and particle volume fraction of the local gas-solid flow. Also, electrostatic and van der Waals forces may cause particles to adhere to both the optical and borescopic probe surfaces, causing significant loss of data. This was particularly a factor in

this study for FCC particles with the optical probe.

- The PEPT and RPT methods rely on the tracer particle travelling in a manner that is perfectly representative of the bulk particles in the bed. However, as seen in Table 3, the diameter and density of the tracer particle used for RPT differed substantially from those of the main particles, with the tracer particle being considerably larger and denser, even belonging to a different Group, B, of the Geldart classification, characterized by different fluidization hydrodynamic features compared to the bulk FCC particles, which belong to Group A. For PEPT measurements, the tracer particle size was well matched, but its density differed significantly. These differences in properties may have affected the measurements, e.g. influencing velocity fluctuations and acceleration, with negative impact on the accuracy of RPT, and, to a lesser extent, the PEPT data. In fact, the terminal velocity of the RPT tracer particle was 5.4 times greater, while that of PEPT tracer was 1.4 times smaller compared to the FCC particles. Better matching of particle/tracer properties in order to assure similar drag forces and acceleration is clearly important when measuring hydrodynamic properties of fluidized beds.
- In order to be accepted as providing valid cross-correlation measurements, particles had to pass the optical probe nearly vertically. No such restriction applies to the PEPT, RPT and borescopic probe techniques.
- The optical probe is incapable of measuring velocities close to 0 because of the need to cross-correlate signals from two fibres. Again this restriction is absent for the other three techniques. Better agreement, especially between the borescope and optical probe radial profiles of time-average solid velocity, was obtained in some cases when particle velocities smaller than 0.023 m/s were excluded from the analysis of signals (Figure 16). PEPT and

RPT also exclude zero-magnitude velocities, since to cross the measurement level and be counted, the tracer must possess a non-zero vertical velocity. As discussed before and observable in the PDFs of solid velocity (Figure 15), the borescope tends to be slightly biased towards nearly-zero velocities, while the method of post-processing adopted with both PEPT and RPT produces results comparable with the optical probe. If instead of the crossing approach, the volume-based method had been used for PEPT and RPT post-processing, the results would have shifted towards velocities of smaller magnitude.

- For PEPT, the average resolution of the system given by location uncertainty was around 3.3 mm, which is of the same order as the distance travelled by the particle during one time step at low particle velocities (<0.06 m/s). This may result in poor accuracy of detecting low solid velocities. An exact theoretical principle for optimising N as a function of particle speed may also be useful for improving the data analysis.
- The four methods have different dependencies on particle volume fraction. In a given time interval, the optical probe returns a particle velocity irrespective of whether there are only a few or many particles passing in the correct direction during that interval. The velocities can therefore be considered to be "volume-fraction-independent". Hence the optical probe is, for example, indifferent to whether the particle is travelling in the dense or dilute phase when it accepts a cross-correlation as giving a valid velocity. The borescope presents a slight volume-fraction dependency since the PIV algorithm needs a sufficient number of particles within the measurement volume. At low particle volume fractions, longer image collections times are needed, resulting in much larger image files (i.e. longer analysis times). Extremely dilute regions provide more freedom of movement in three-dimensional space, resulting in cases where particles present in one frame escape from the field of view

in the next frame. Otherwise, the borescope dependency on volume fraction is weak since, providing there are some particles within the measuring volume, their number is not important. On the other hand, in the RPT and PEPT methods, over long time periods, the tracer particle passes more times through regions of high flux than in low-flux regions. Thus the measurements may be more accurate in high-flux regions because of averaging over more data, but the values over long time periods should be "flux independent". If we compare optical and borescopic probes, the borescope has a significantly larger measuring volume, resulting in some spatial averaging that is not a consideration for the optical probe. Also, the detection of movement of particles far from the tip of the borescope is difficult because of the short focal length. This happens mostly when dilute phase passes the borescope, and is less of a factor for the optical probe, which relies on the intensity of reflected light, and to a much lesser extent on focus.

- FCC particles tended to adhere to probes, as noted above. Perhaps as a result, the FCC particles gave low optical fibre correlation coefficients, with 35% valid data, compared to 65% for sand. Worse matching between the optical fibre diameter and particle diameter for the FCC may also have been a contributing factor.
- Friction along the tip of the borescope and optical probe may also have restrained particle movement.
- Considering all of these factors and the significant differences among the quantitative data, it is clear that none of the experimental techniques is perfect. Experimental limitations need to be considered when comparing predictions of CFD and other models with experimental measurements.

5.0 Conclusions

Optical fibre probes, radioactive particle tracking, positron emission particle tracking and borescopic high-speed PIV were deployed to investigate local particle velocities in a "traveling fluidized bed" operated under identical conditions at four locations with the same FCC particles (Geldart Group A powder). Fair agreement among the results of the four experimental techniques was found, but there were some significant quantitative differences. Likely reasons for these discrepancies include invasiveness of two of the methods, differences between the physical properties of tracer particles and the bulk bed material, different sensitivities to the angle of travel and concentration of particles in the measurement zone, unequal measurement volumes, and differences in acceptance algorithms. Analysis of the data leads to valuable insights on the merits and physical features of each of the measurement techniques. For most cases examined, the data obtained by RPT, borescopy and optical probes and, to a lesser extent, PEPT presented fair agreement with each other, delineating the range of solid velocities to be expected in this system at different superficial gas velocities. Therefore, the results of this study help to provide an experimental hydrodynamic database useful for testing the validity of CFD and other models.

Acknowledgement

The authors are grateful to the Natural Sciences and Engineering Research Council of Canada for an RTI grant, which made it possible to build the equipment, and for Discovery grant funding which assisted in supporting graduate students and in covering transportation and operation of the equipment. We also acknowledge help from Coanda Research & Development in designing, constructing and commissioning the traveling experimental facility.

Nomenclature

d_{sauter}	Sauter mean particle diameter, μm
d_{fibre}	external diameter of optical probe fibres, μm
d_{probe}	external diameter of optical probe, mm
E	error of cross-correlation, m/s
f	sampling frequency necessary for optical probes, Hz
f_{opt}	final fraction of γ-ray sample, -
I_p	interval of measurable velocities using optical probe, m/s
I_w	interval of measurable velocities in wall region using optical probe, m/s
L_e	effective distance between receiving ends of optical probe, m
M	multiplicand for time-lag, -
m_s	minimum distance point, mm
N	initial sample size, -
$\vec{P}_i$	PEPT tracer particle location vector, mm
T_{int}	integration time, s
U_c	superficial gas velocity at transition to turbulent flow regime, m/s
v_p	local instantaneous particle velocity, m/s
$v_{p,min}$	minimum particle velocity measurable by optical probe, m/s
$v_{p,max}$	maximum particle velocity measurable by optical probe, m/s
$v_{p,x}$, $v_{p,y}$, $v_{p,z}$	coordinates of instantaneous vector of tracer particle velocity, m/s
w	positron camera resolution, mm
x,y,z	spatial coordinates of instantaneous tracer position, m
Δ	location precision for PEPT, mm

ρ gas density, kg/m^3

ρ_p particle density, kg/m^3

τ_l time-lag between two signals of optical probes, s

References

Cocco, R., Shaffer, F., Hays, R., Reddy Karri, S.B., Knowlton, T., 2010. Particle clusters in and above fluidized beds. Powder Technol. 203, 3–11. doi:10.1016/j.powtec.2010.03.023

Dubrawski, K., Tebianian, S., Bi, H.T., Chaouki, J., Ellis, N., Gerspacher, R., Jafari, R., Kantzas, A., Lim, C., Patience, G.S., Pugsley, T., Qi, M.Z., Zhu, J.X., Grace, J.R., 2013. Traveling column for comparison of invasive and non-invasive fluidization voidage measurement techniques. Powder Technol. 235, 203–220. doi:10.1016/j.powtec.2012.10.031

Ellis, N., 2003. Hydrodynamics of Gas-Solid Turbulent Fluidized Beds. University of British Columbia, Vancouver, Canada.

Grace, J.R., Taghipour, F., 2004. Verification and validation of CFD models and dynamic similarity for fluidized beds. Powder Technol. 139, 99–110. doi:10.1016/j.powtec.2003.10.006

Herbert, P.M., Gauthier, T.A., Briens, C.L., Bergougnou, M.A., 1994. Application of fiber optic reflection probes to the measurement of local particle velocity and concentration in gas—solid flow. Powder Technol. 80, 243–252. doi:10.1016/0032-5910(94)02859-1

Kunii, D., Levenspiel, O., 1991. Fluidization Engineering. Butterworth-Heinemann.

Larachi, F., Chaouki, J., Kennedy, G., Dudukovic, M.P., 1996. Radioactive particle tracking in multiphase reactors: principles and applications, in: J. Chaouki, F. Larachi, M.P. Dudukovic (Eds.), Non-Invasive Monitoring of Multiphase Flows 335–405.

Leadbeater, T., Parker, D.J., 2013. Current trends in positron emission particle tracking, in: Proceedings of 7th World Congress on Industrial Process Tomography. Presented at the WCIPT7, Elsevier, Krakow, Poland.

Leadbeater, T.W., Parker, D.J., Gargiuli, J., 2012. Positron imaging systems for studying particulate, granular and multiphase flows. Particuology, Advances in Characterization and Modeling of Particulate Processes 10, 146–153. doi:10.1016/j.partic.2011.09.006

Liu, J., Grace, J.R., Bi, X., 2003. Novel multifunctional optical-fiber probe: I. Development and validation. AIChE J. 49, 1405–1420. doi:10.1002/aic.690490607

Lyczkowski, R.W., Gamwo, I.K., Dobran, F., Ai, Y.H., Chao, B.T., Chen, M.M., Gidaspow, D., 1993. Validation of computed solids hydrodynamics and pressure oscillations in a bubbling atmospheric fluidized bed. Powder Technol. 76, 65–77. doi:10.1016/0032-5910(93)80042-9

Nguyen, H.V., Whitehead, A.B., Potter, O.E., 1977. Gas backmixing, solids movement, and bubble activities in large scale fluidized beds. AIChE J. 23, 913–922. doi:10.1002/aic.690230619

Raffel, M., Willert, C., Kompenhans, J., 1998. Particle Image Velocimetry, A Practical Guide Springer. N. Y.

Stein, M., Martin, T.W., Seville, J.K., McNeil, P.A., Parker, D.J., 1996. Positron emission particle tracking: Particle velocities in gas-fluidised beds, mixers and other applications, in: J. Chaouki, F. Larachi, M.P. Dudukovic (Eds.), Non-Invasive Monitoring of Multiphase Flows 309–333.

Thielicke, W., 2013. Personal communication. http://pivlab.blogspot.ca/.

Van Ommen, J.R., Mudde, R.F., 2008. Measuring the Gas-Solids Distribution in Fluidized Beds–

A Review. Int. J. Chem. React. Eng. 6.

Werther, J., 1999. Measurement techniques in fluidized beds. Powder Technol. 102, 15–36. doi:10.1016/S0032-5910(98)00202-2

Yang, W.-C., 2003. Bubbling Fluidized Beds, in: W-C. Yang (Ed.), Handbook of Fluidization and Fluid-Particle Systems, Marcel Dekker, Inc., New York.

Yates, J.G., Simons, S.J.R., 1994. Experimental methods in fluidization research. Int. J. Multiph. Flow 20, Supplement 1, 297–330. doi:10.1016/0301-9322(94)90076-0

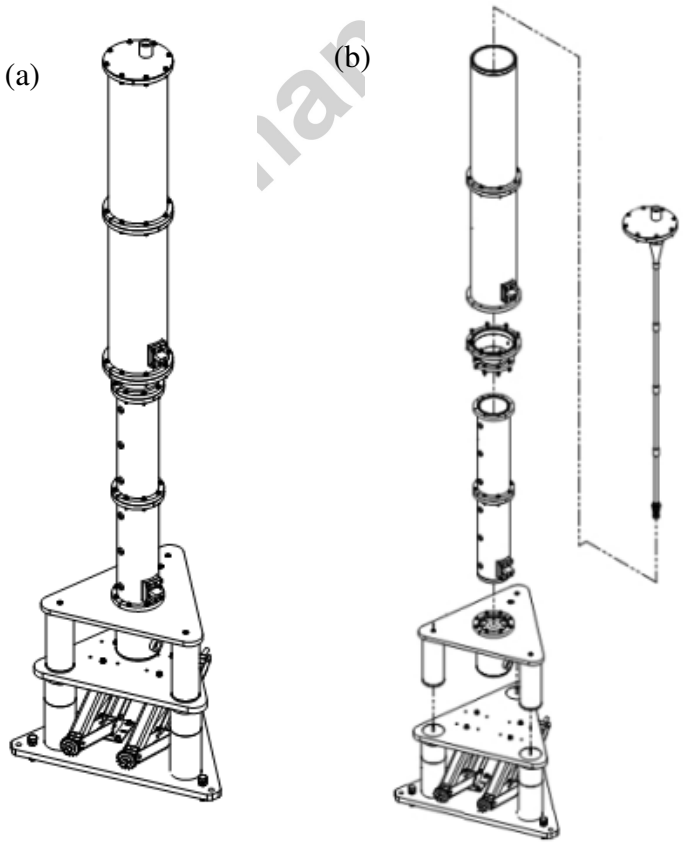

Figure 1-Traveling fluidized bed (TFB) column: a) assembled; b) exploded modular view.

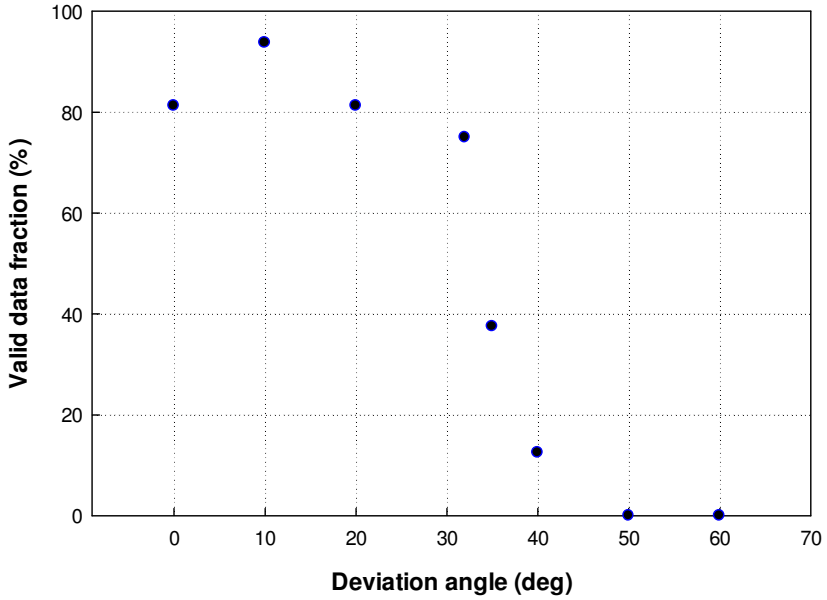

Figure 2 – Sensitivity to measurement angle of optical probe

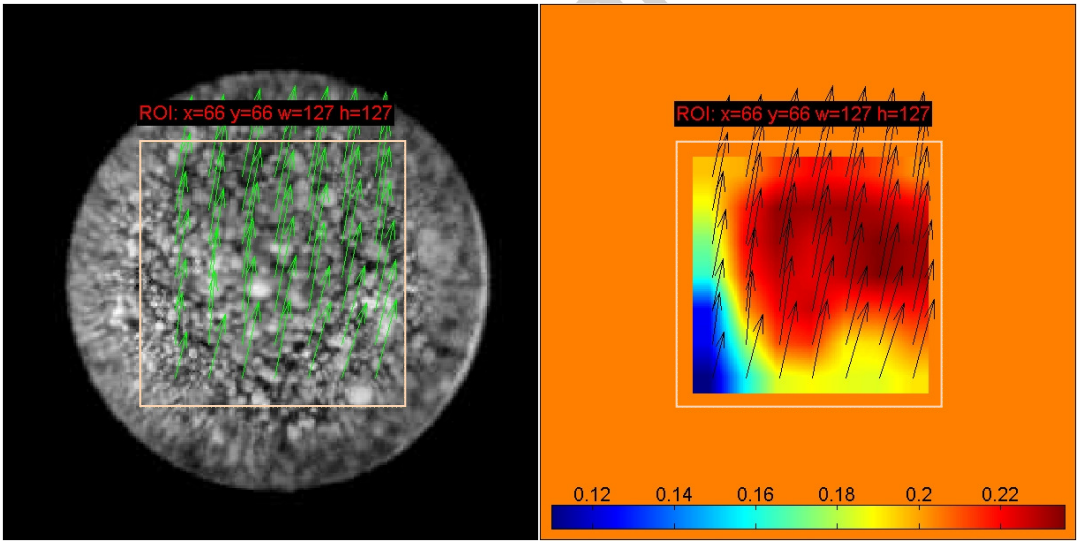

Figure 3 – Velocity vectors obtained by PIVlab in a region of interest for FCC particles

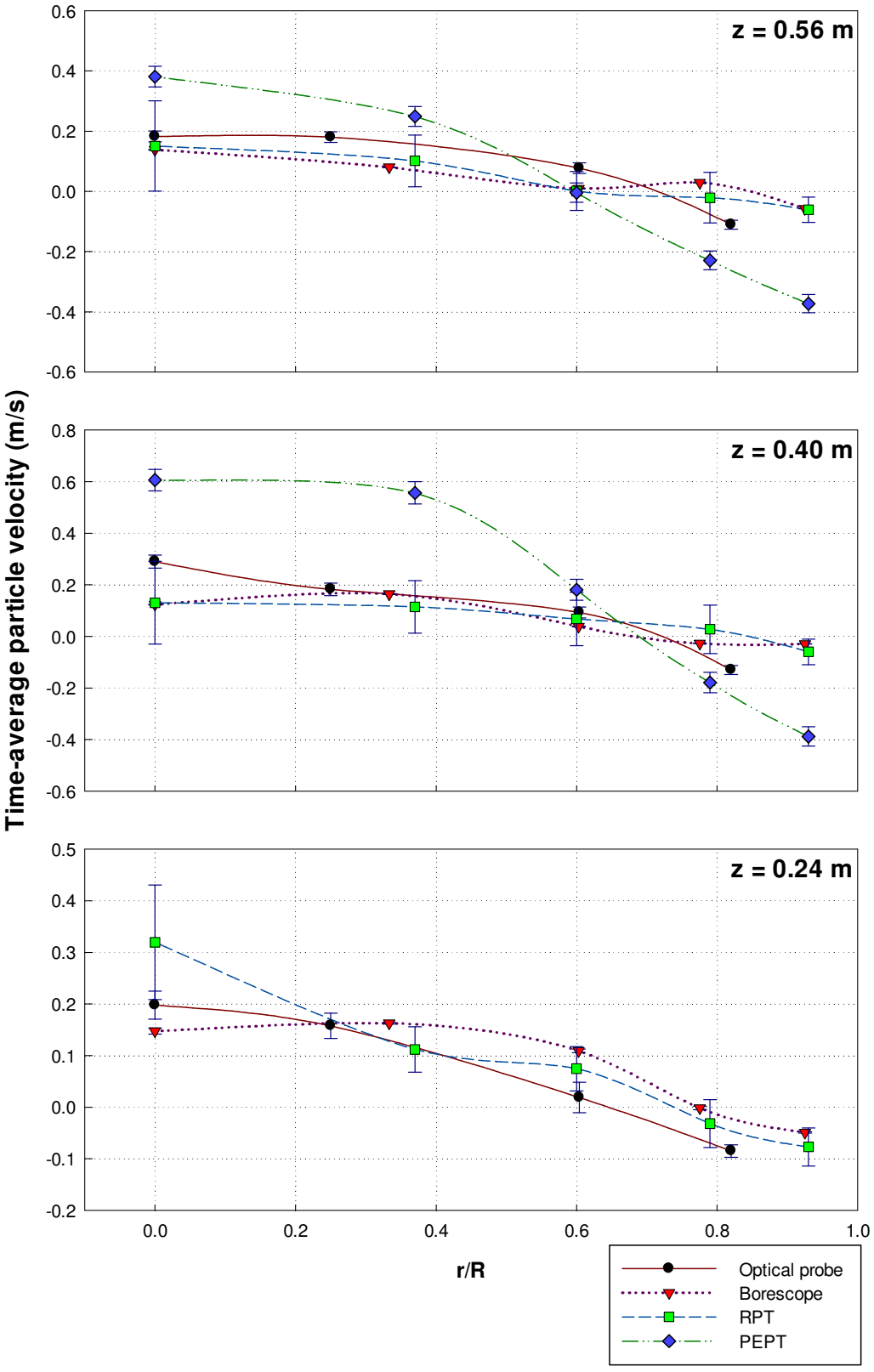

Figure 4 – Radial profiles of time-average solid velocity at three levels for FCC, U_g = 0.30 m/s.

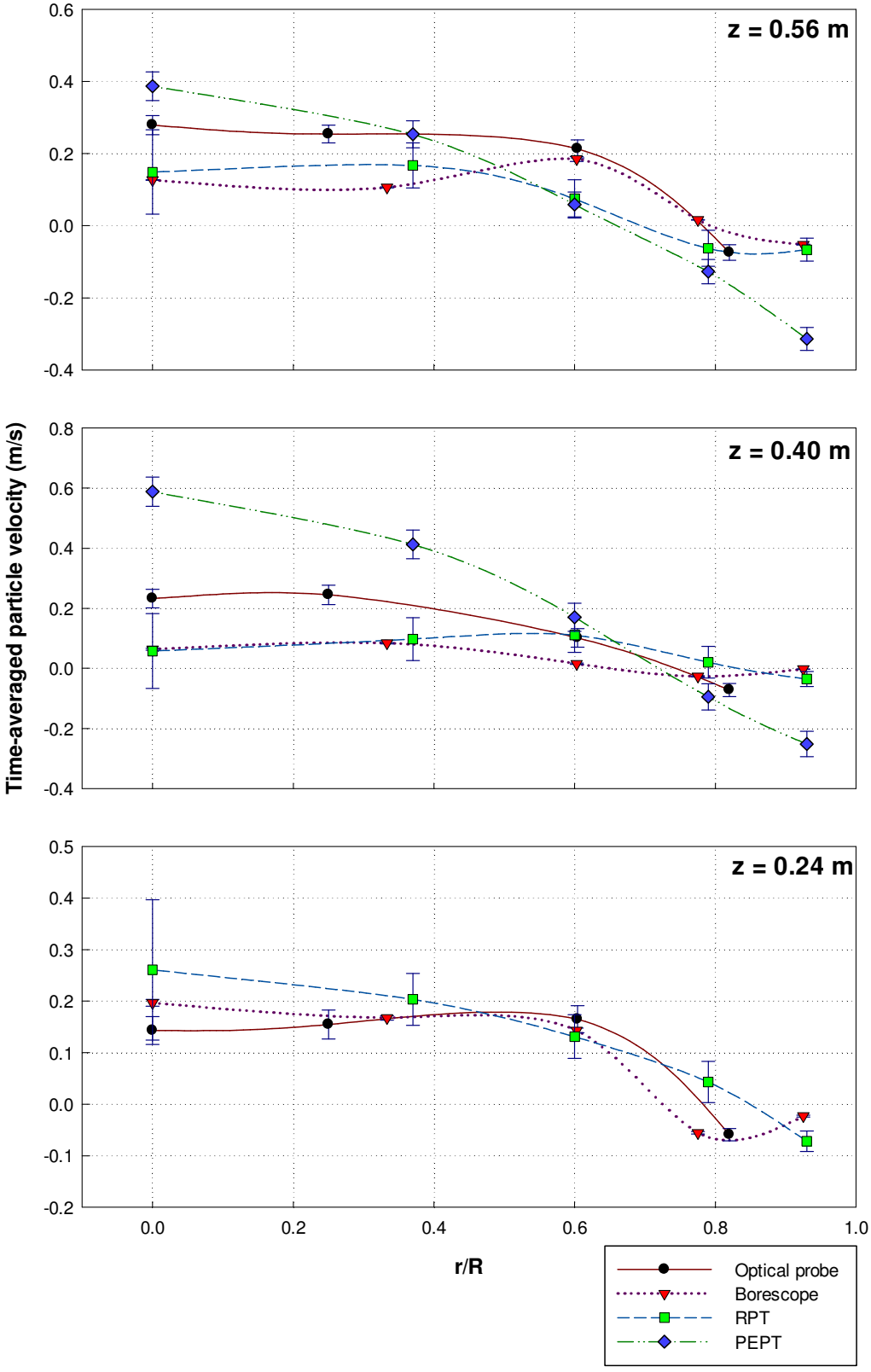

Figure 5 – Radial profiles of time-average solid velocity at three levels for FCC, U_g = 0.40 m/s

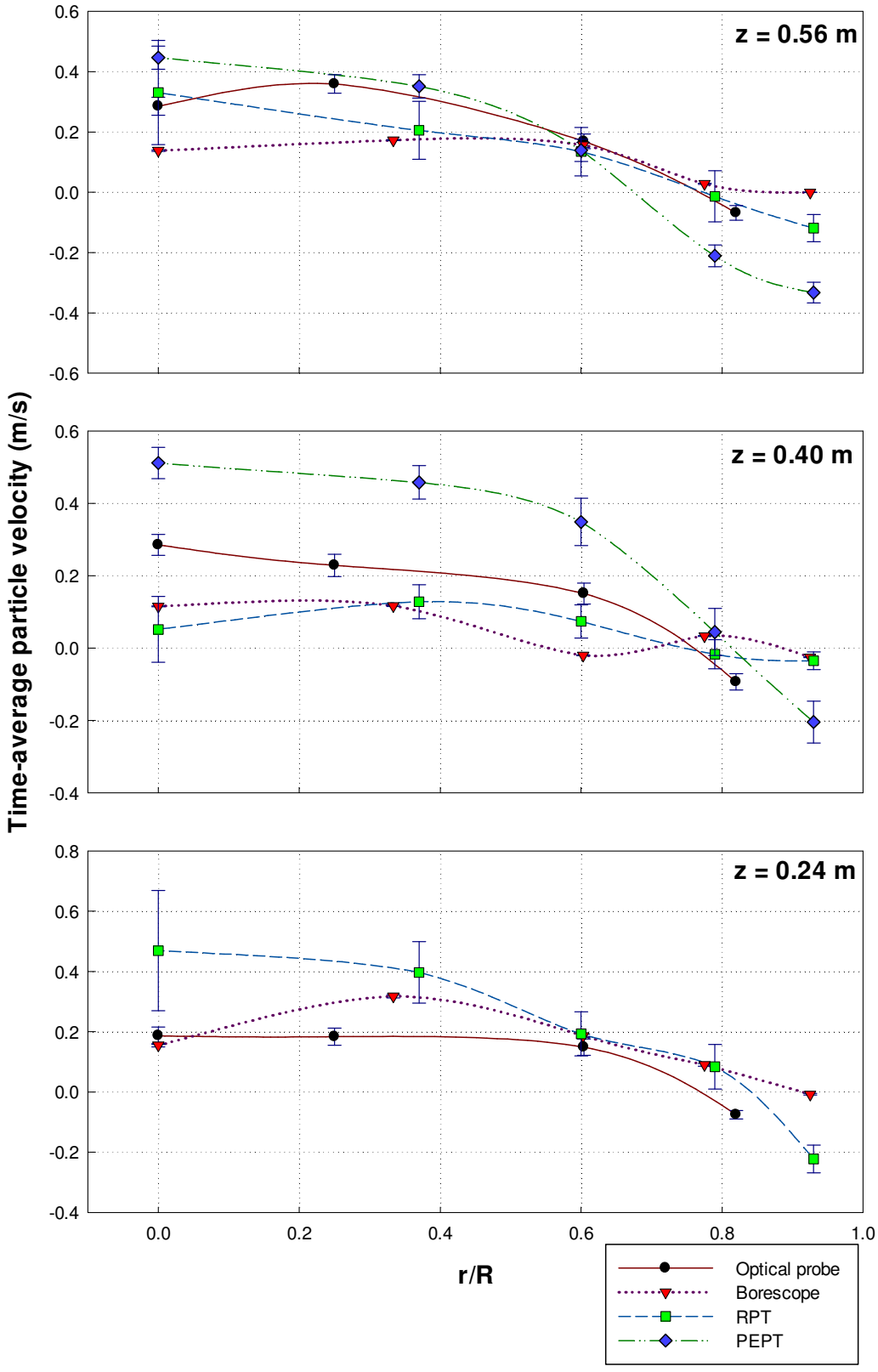

Figure 6 – Radial profiles of time-average solid velocity at three levels for FCC, U_g = 0.50 m/s

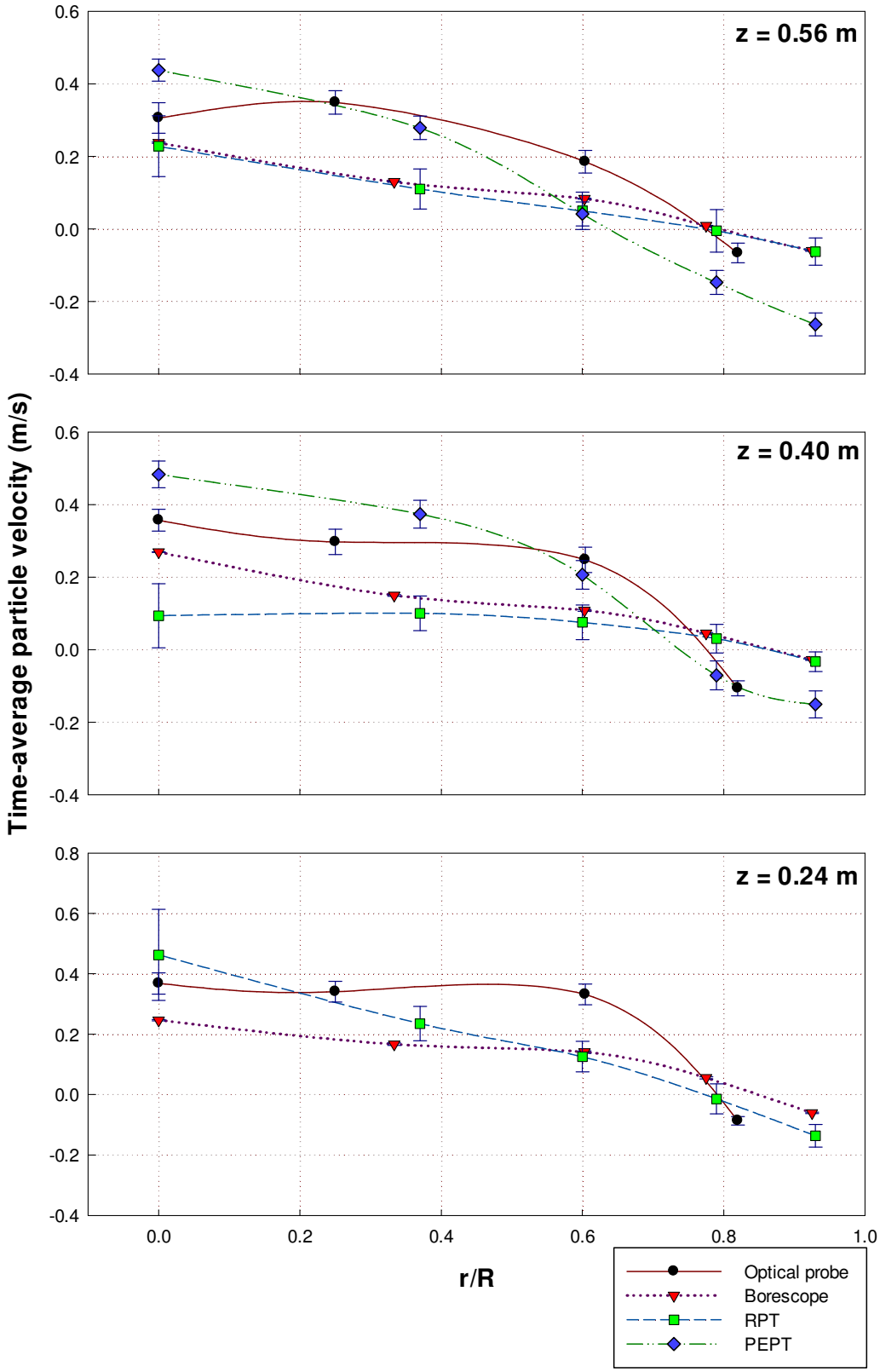

Figure 7 – Radial profiles of time-average solid velocity at three levels for FCC, U_g = 0.60 m/s

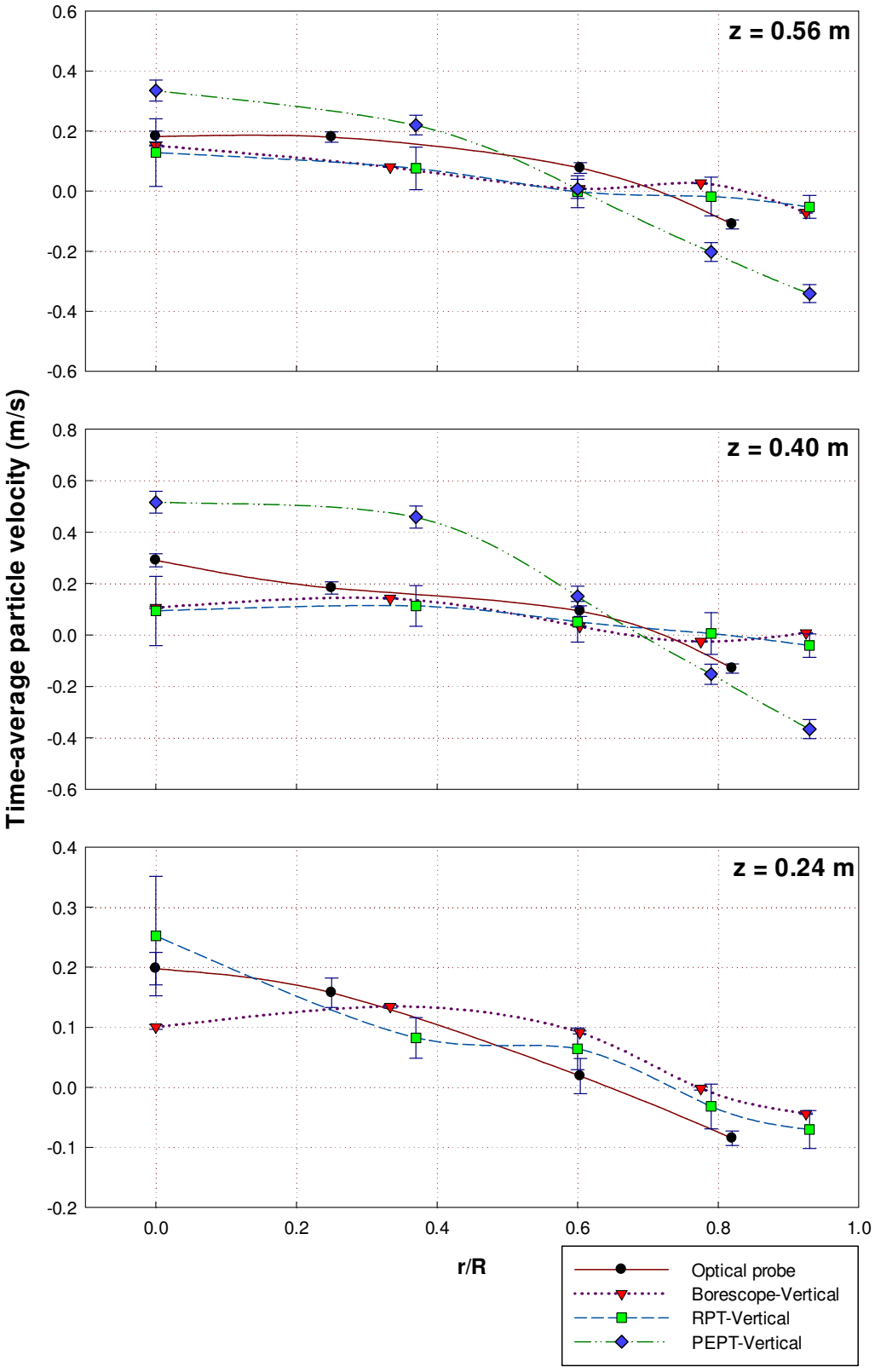

Figure 8 – Radial profiles of time-average solid velocity at three levels for FCC based on vertical components of velocity vectors, U_g = 0.30 m/s

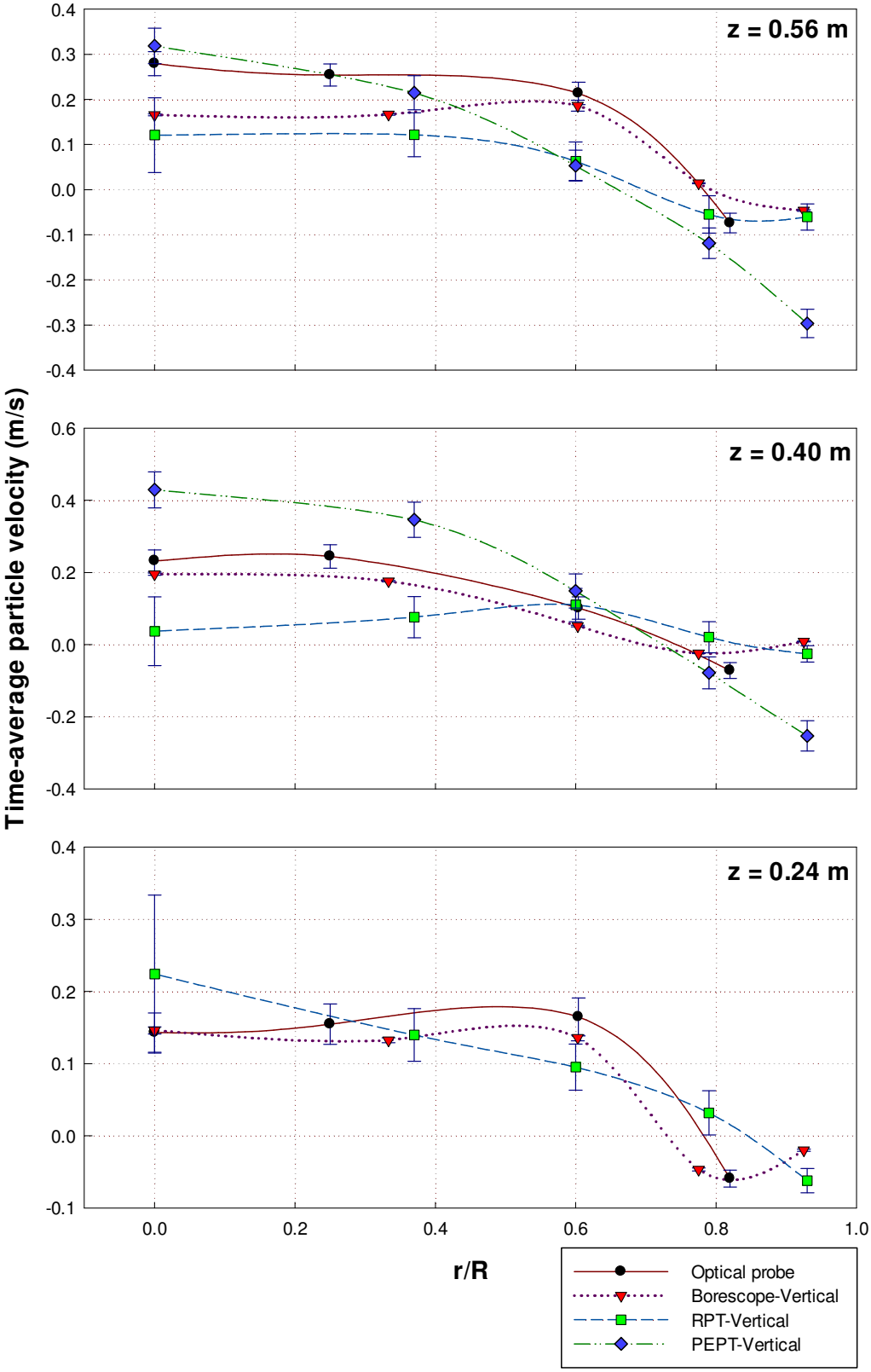

Figure 9 – Radial profiles of time-average solid velocity at three levels for FCC based on vertical components of velocity vectors, U_g = 0.40 m/s

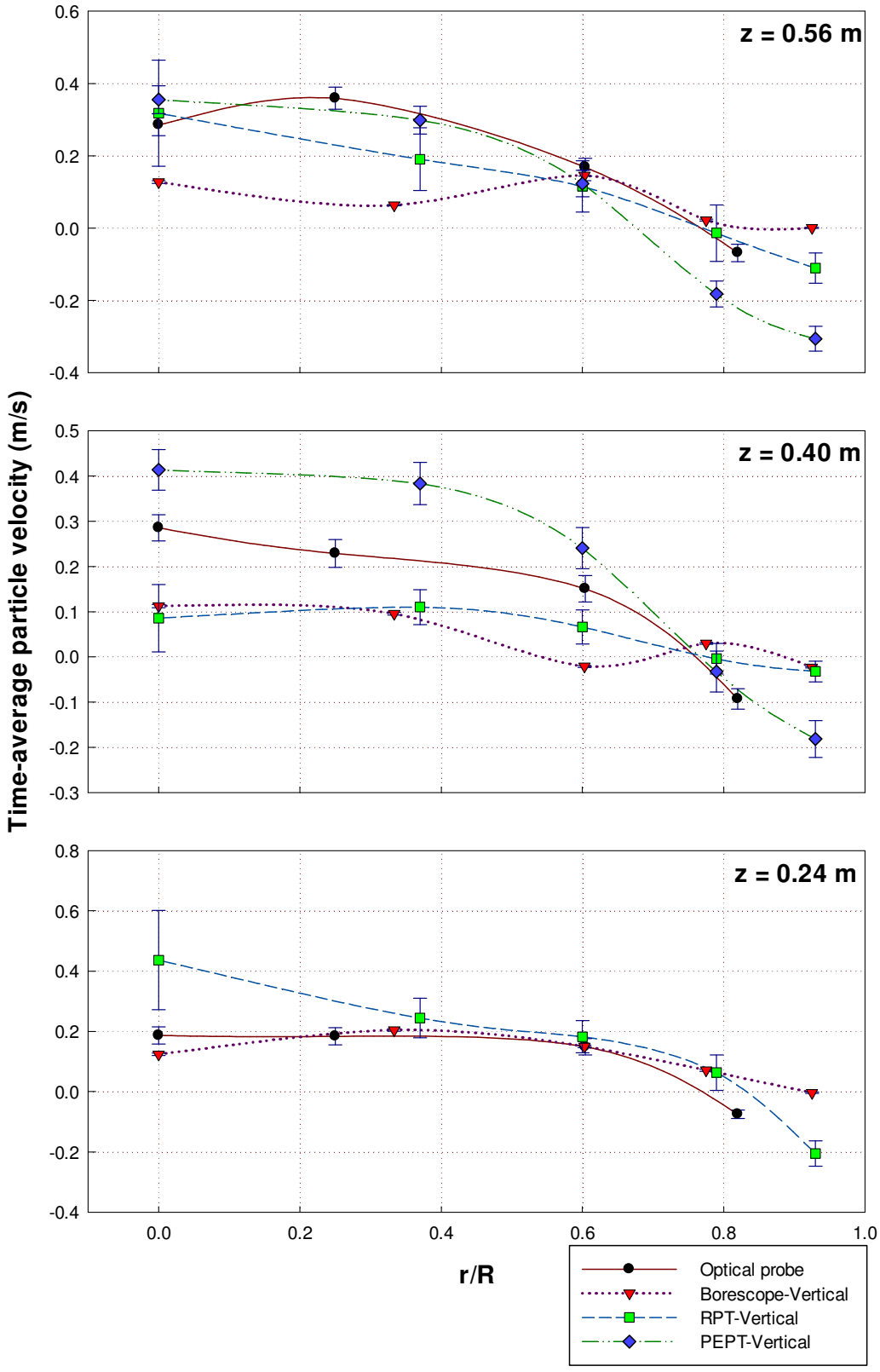

Figure 10 – Radial profiles of time-average solid velocity at three levels for FCC based on vertical components of velocity vectors, U_g = 0.50 m/s

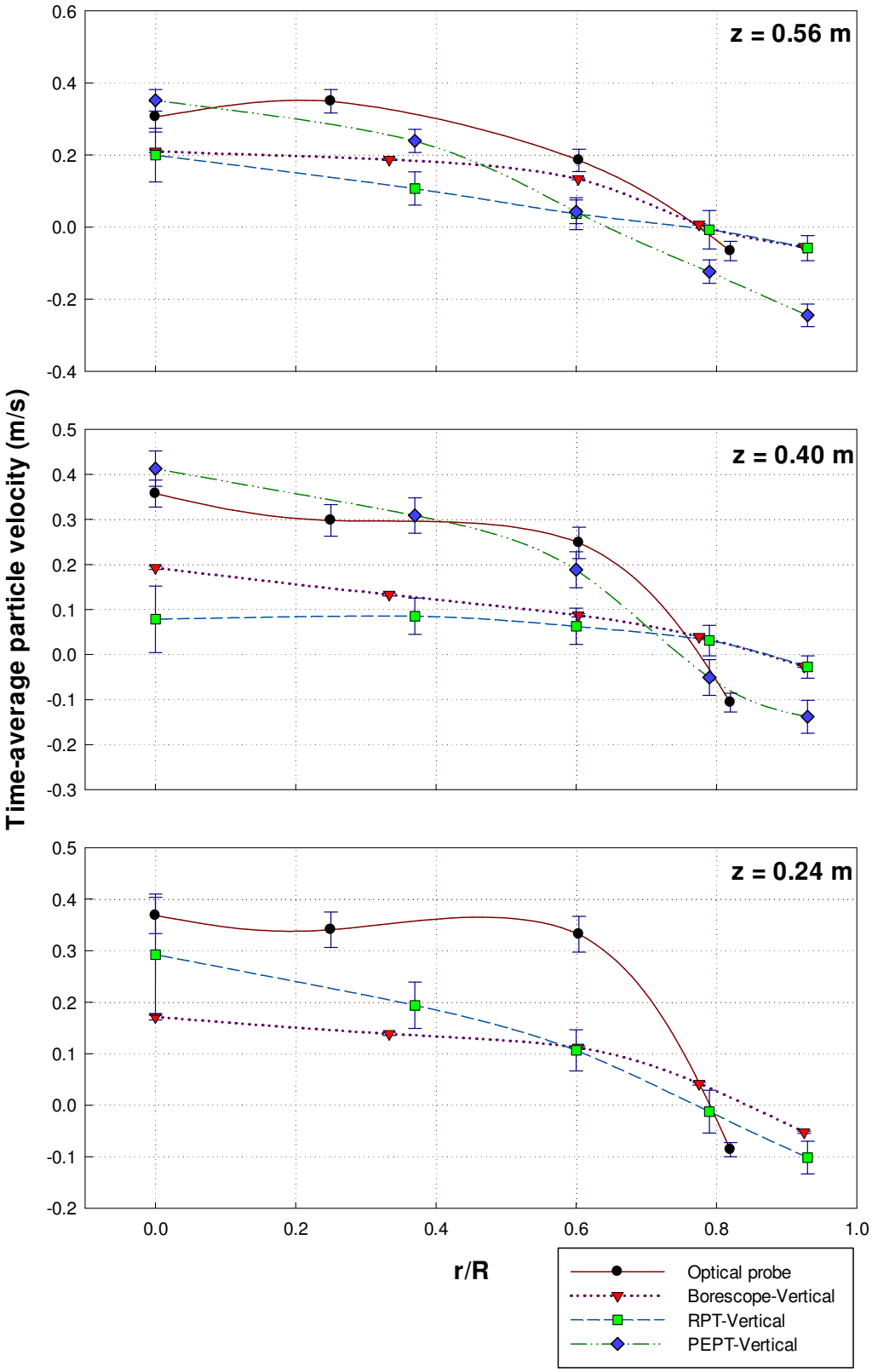

Figure 11 – Radial profiles of time-average solid velocity at three levels for FCC based on vertical components of velocity vectors, U_g = 0.60 m/s

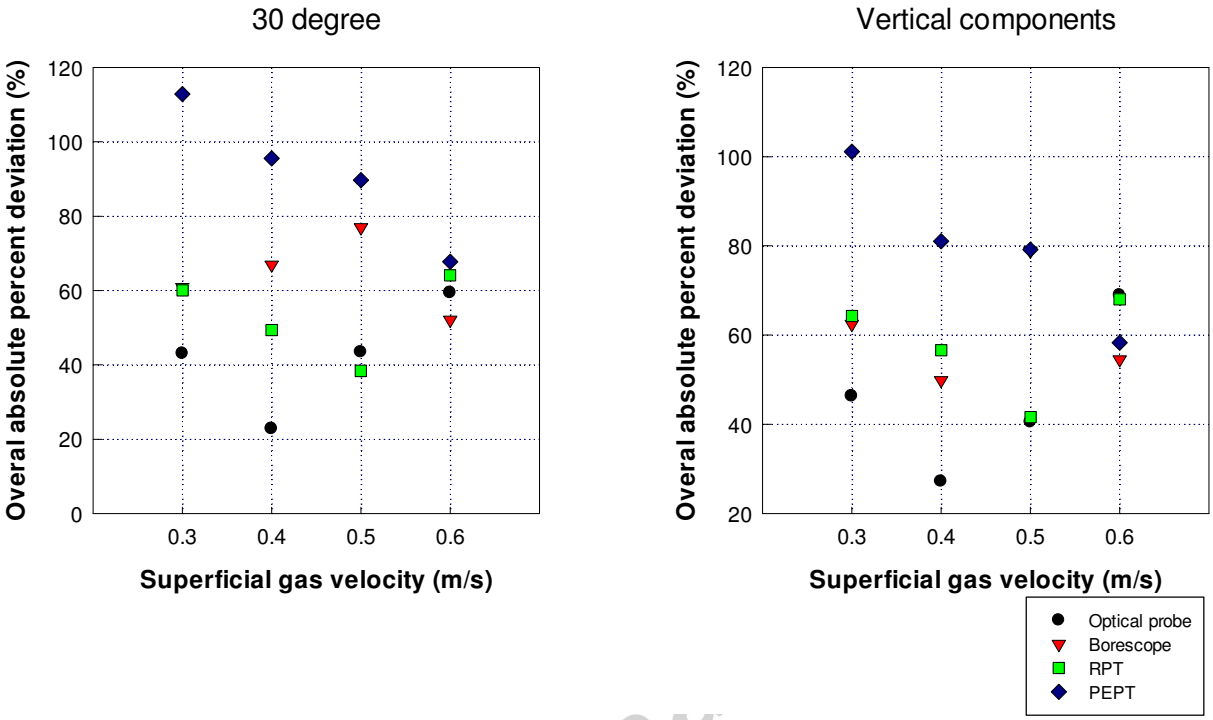

Figure 12 – Overall percent deviation for different superficial gas velocities. Considering: a) Velocities with a deviation angle of less than 30 degrees from the vertical; b) Vertical components of the velocities

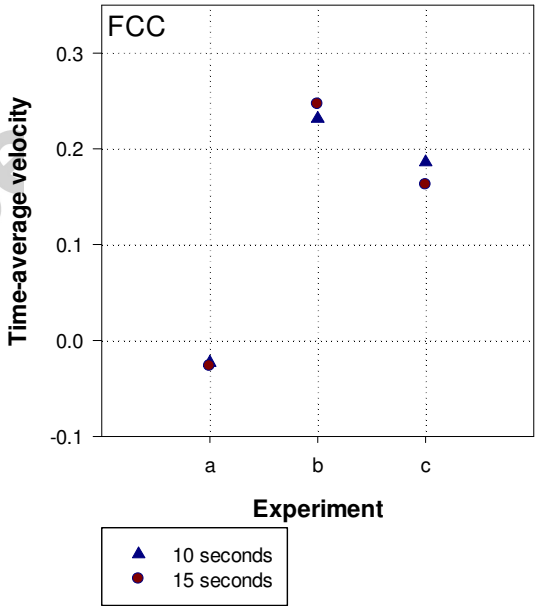

Figure 13 – Effect of the sampling time on the time-averaged particle velocity measured by the borescope. FCC: a) U_g = 0.40 m/s, z=0.4m, r/R=0.77; b) U_g = 0.60 m/s, z=0.4m, r/R=0; c) U_g = 0.30 m/s, z=0.24m, r/R=0.33

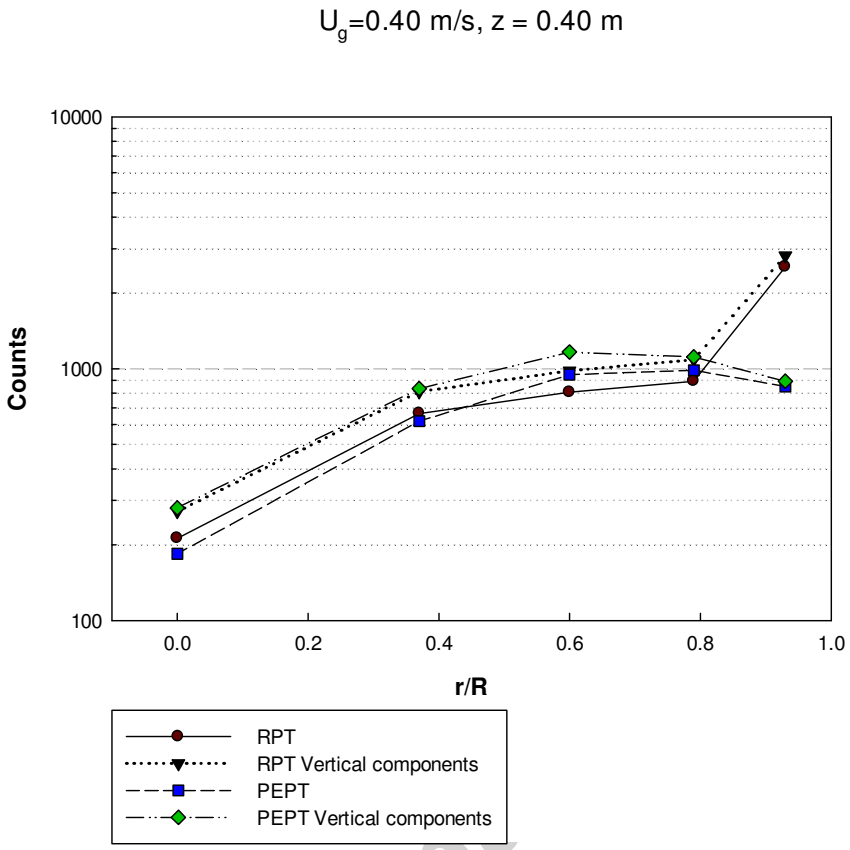

Figure 14 - Count number for RPT and PEPT in different annuli with different filtering criteria, U_g = 0.40 m/s, z = 0.40 m

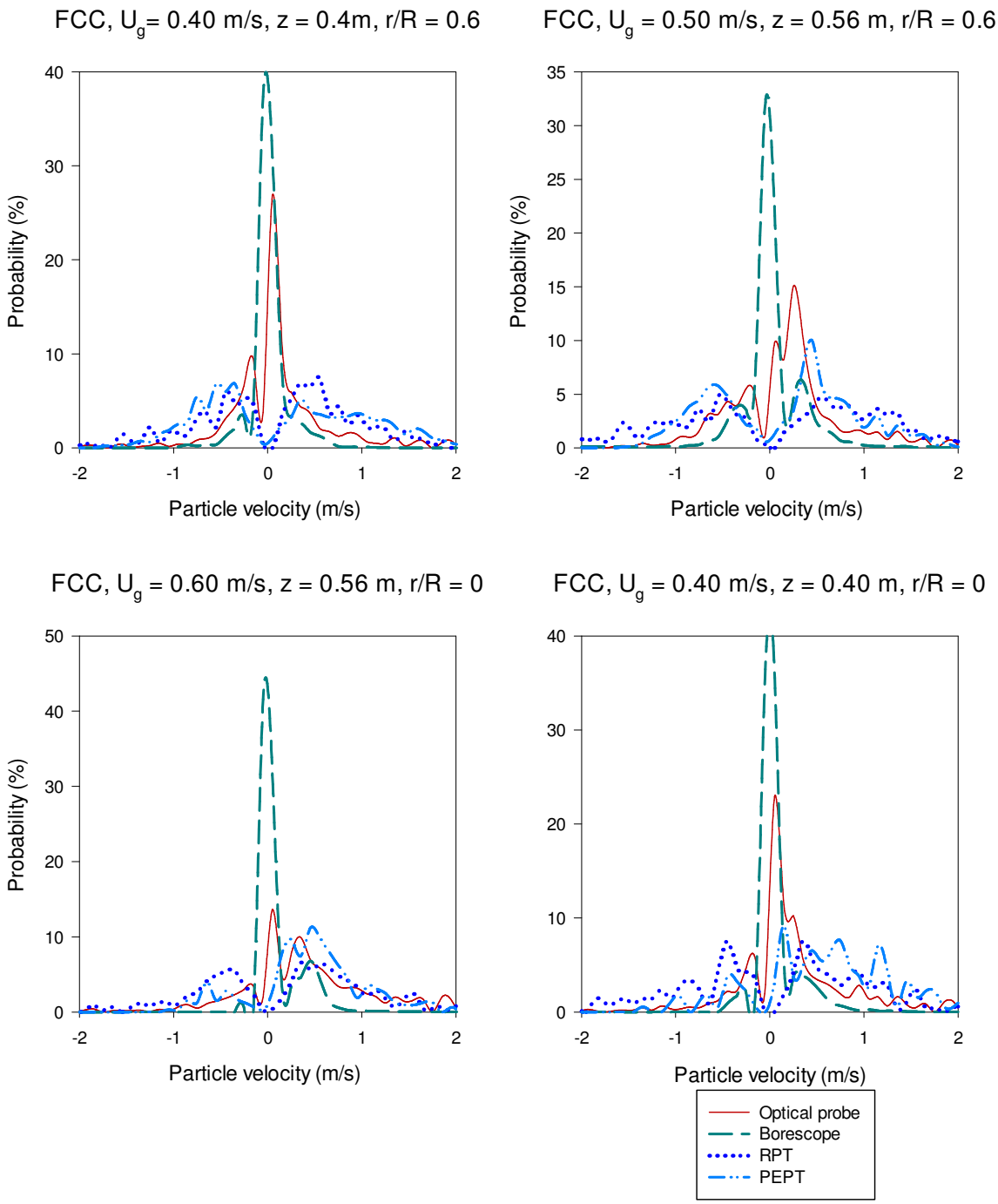

Figure 15 – Examples of probability distribution function of solid velocity

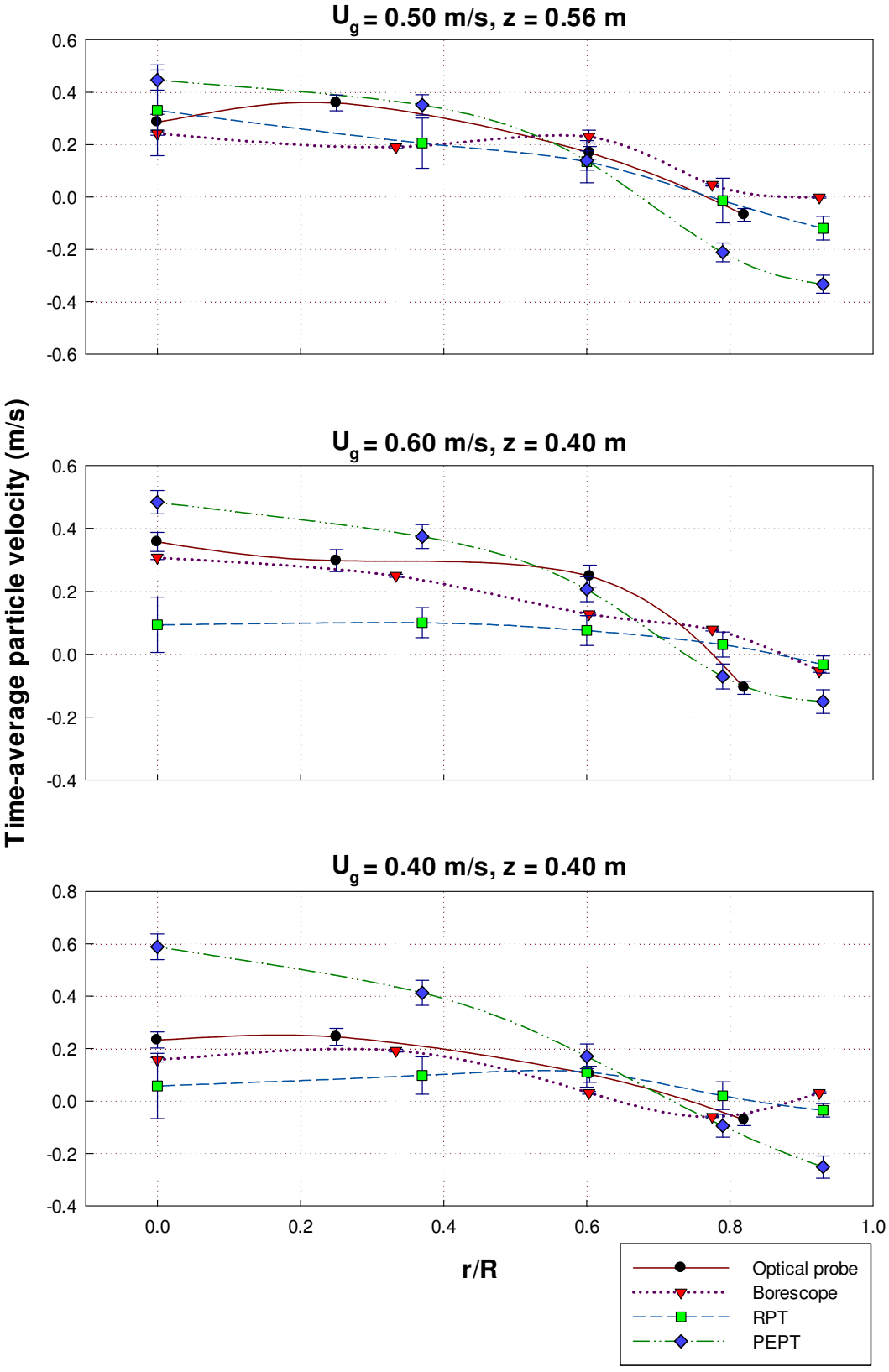

Figure 16 – Radial profiles of time-average solid velocity at three levels for FCC excluding zero velocities

- A novel travelling fluidized bed was built to ensure identical operating conditions
- The equipment traveled to different laboratories for hydrodynamic investigation
- The most advanced particle velocity measurement techniques are directly compared
- The reasons underlying observed discrepancies among the results are discussed
- A comprehensive experimental database for model testing is extended